A&A 455, 1059–1072 (2006)
DOI: 10.1051/0004-6361:20064802

Astronomy & Astrophysics

CS 30322-023: an ultra metal-poor TP-AGB star?⋆

T. Masseron[1], S. Van Eck[2], B. Famaey[2], S. Goriely[2], B. Plez[1], L. Siess[2], T. C. Beers[3], F. Primas[4], and A. Jorissen[2]

[1] GRAAL, UMR 5024 CNRS, Université de Montpellier-II, France
e-mail: ajorisse@astro.ulb.ac.be
[2] Institut d'Astronomie et d'Astrophysique, Université Libre de Bruxelles, CP 226, Boulevard du Triomphe, 1050 Bruxelles, Belgium
[3] Department of Physics and Astronomy, Center for the Study of Cosmic Evolution (CSCE) and Joint Institute for Nuclear Astrophysics (JINA), Michigan State University, East Lansing, MI 48824-1116, USA
[4] European Southern Observatory, K. Schwarzschild Straße 2, 85748 Garching bei München, Germany

Received 3 January 2006 / Accepted 5 May 2006

ABSTRACT

Context. The remarkable properties of CS 30322-023 became apparent during the course of a high-resolution spectroscopic study of a sample of 23 carbon-enhanced, metal-poor (CEMP) stars.
Aims. This sample is studied in order to gain a better understanding of s- and r-process nucleosynthesis at low metallicity, and to investigate the role of duplicity.
Methods. High-resolution UVES spectra have been obtained, and abundances are derived using 1-D, plane-parallel OSMARCS models under the LTE hypothesis. The derived atmospheric parameters and observed abundances are compared to evolutionary tracks and nucleosynthesis predictions to infer the evolutionary status of CS 30322-023.
Results. CS 30322-023 is remarkable in having the lowest surface gravity ($\log g \leq -0.3$) among the metal-poor stars studied to date. As a result of its rather low temperature (4100 K), abundances could be derived for 35 chemical elements; the abundance pattern of CS 30322-023 is one of the most well-specified of all known extremely metal-poor stars. With [Fe/H] = −3.5, CS 30322-023 is the most metal-poor star to exhibit a clear s-process signature, and the most metal-poor "lead star" known. The available evidence indicates that CS 30322-023 is presently a thermally-pulsing asymptotic giant branch (TP-AGB) star, with no strong indication of binarity thus far (although a signal of period 192 d is clearly present in the radial-velocity data, this is likely due to pulsation of the stellar envelope). Low-mass TP-AGB stars are not expected to be exceedingly rare in a magnitude-limited sample such as the HK survey, because their high luminosities make it possible to sample them over a very large volume. The strong N overabundance and the low $^{12}C/^{13}C$ ratio (4) in this star is typical of the operation of the CN cycle. Coupled with a Na overabundance and the absence of a strong C overabundance, this pattern seems to imply that hot-bottom burning operated in this star, which should then have a mass of at least 2 $M_\odot$. However, the luminosity associated with this mass would put the star at a distance of about 50 kpc, in the outskirts of the galactic halo, where no recent star formation is expected to have taken place. We explore alternative scenarios in which the observed abundance pattern results from some mixing mechanism yet to be identified occurring in a single low-metallicity 0.8 $M_\odot$ AGB star, or from pollution by matter from an intermediate-mass AGB companion which has undergone hot-bottom burning. We stress, however, that our abundances may be subject to uncertainties due to NLTE or 3D granulation effects which were not taken into consideration.

Key words. stars: AGB and post-AGB – stars: carbon – stars: evolution – stars: individual: CS 30322-023 – Galaxy: halo

1. Introduction

The star CS 30322-023 first appeared in the Norris et al. (1999) list of broadband photometry for candidate metal-poor stars selected from the HK survey (Beers et al. 1985, 1992). Follow-up medium-resolution spectroscopy of CS 30322-023 revealed that it was likely to be rather C-rich. It was therefore included in our sample of 23 carbon-enhanced metal-poor (CEMP) stars observed with the UVES spectrograph on VLT-Kueyen, in order to look for more lead stars after the initial discoveries by Van Eck et al. (2001, 2003). Lead stars are low-metallicity objects where the operation of the s-process nucleosynthesis was so efficient that it converted a relatively large fraction of iron-seed nuclei all the way to lead (Goriely & Mowlavi 2000). The sample we investigated was collected from three different sources:

- CEMP objects from the HK survey not included in high-resolution follow-up studies by other teams;
- stars from the list of faint high-latitude carbon stars in the Hamburg-ESO (HE) survey (Christlieb et al. 2001) which have strong CN or C_2 bands;
- the catalogue of low-metallicity stars with strong CH bands from Šleivyte & Bartkevičius (1990).

Preliminary analyses of this sample have been presented by Masseron et al. (2005, 2006); a more detailed paper is in preparation as part of Masseron's Ph.D. thesis (*Observatoire de Paris*, France).

The star CS 30322-023 deserves, however, a dedicated analysis, as it exhibits several pecularities as compared to other metal-poor stars. First, as will be shown in Sect. 6, it is another

⋆ Based on observations performed with the Very Large Telescope at the European Southern Observatory, Paranal, Chile, under programs 69.D-0063(A), 73.D-0193(A,B), 74.D-0228(A), 75.D-0120(A), 76.D-0451(A), 165.N-0276(A).

Table 1. Observation log. The uncertainty on the radial-velocity Vr arising from the template mismatch ($\epsilon_{\rm temp}$), from the Gaussian fit of the correlation profile ($\epsilon_{\rm fit}$), and their root-mean-square ($\epsilon_{\rm tot}$), are also listed.

Date (YYYY/MM/DD)	HJD (–2 450 000)	Exp. time (s)	Vr (km s^{-1})	$\epsilon_{\rm temp}$ (km s^{-1})	$\epsilon_{\rm fit}$ (km s^{-1})	$\epsilon_{\rm tot}$ (km s^{-1})	Telescope	Programme
2001/11/04	2218.49762	3100	116.53[a]	–	0.08	0.08	VLT/UVES	165.N-0276(A)
2002/04/24	2388.83689	3600	116.40	0.04	0.04	0.06	VLT/UVES	069.D-0063(A)
2002/05/11	2405.86677	3600	114.59	0.05	0.04	0.06	VLT/UVES	069.D-0063(A)
2004/04/29	3124.92121	90	115.92	0.04	0.04	0.06	VLT/UVES	073.D-0193(B)
2004/06/14	3170.81670	90	115.75	0.04	0.03	0.05	VLT/UVES	073.D-0193(B)
2004/08/17	3234.64390	90	112.81	0.05	0.02	0.05	VLT/UVES	074.D-0228(A)
2004/11/11	3320.53675	90	115.71	0.05	0.03	0.06	VLT/UVES	074.D-0228(A)
2005/06/29	3550.89234	900	115.09[b]	0.37	0.05	0.37	2.2m/FEROS	075.D-0120(A)
2005/07/26	3577.86729	900	114.61[b]	0.39	0.08	0.40	2.2m/FEROS	075.D-0120(A)
2005/07/27	3578.81266	900	113.69[b]	0.29	0.09	0.30	2.2m/FEROS	075.D-0120(A)
2005/07/28	3579.89378	900	113.82[b]	0.61	0.08	0.61	2.2m/FEROS	075.D-0120(A)
2005/08/17	3599.67995	2000	113.35[c]	0.03	0.05	0.06	VLT/UVES	076.D-0451(A)

[a] Data kindly communicated by M. Spite.
[b] Data kindly communicated by S. Lucatello.
[c] Data kindly communicated by J. Johnson.

example of a lead star. Secondly, despite the presence of a definite, albeit moderate, s-process signature, it has almost no C enhancement, the strength of the CN bands being due to a strong N overabundance. It is therefore one of the few known Nitrogen-Enhanced Metal-Poor (NEMP) stars. Thirdly, its most intriguing property is, by far, its very low gravity ($\log g$ about -0.3), coupled with a rather low temperature (4100 K; Sect. 3). Its evolutionary status is thus puzzling (Sect. 4); is it a low-mass ($\sim$0.8 $M_\odot$) star close to the tip of the AGB or a rather luminous intermediate-mass star located in the outskirts of the galactic halo? Either possibility raises intriguing questions concerning its nature, which are addressed in Sects. 5 and 7. Among these are: what is the probability of catching a low-mass star in an evolutionary stage so close to the tip of the AGB? Is the star formation history in the halo consistent with late formation of an extremely low-metallicity intermediate-mass star in the outskirsts of the Galaxy? Is it a star accreted during a merger event with a satellite galaxy? Is it a star that evaporated from a globular cluster? Is it a low-mass star polluted by an intermediate-mass companion formerly on the thermally-pulsing aymptotic giant branch?

2. Observations and radial-velocity variations

Several high-resolution spectra of CS 30322-023 have been obtained at the European Southern Observatory with the UVES spectrograph mounted on the VLT-Kueyen telescope, and with the FEROS spectrograph mounted on the 2.2 m telescope (courtesy S. Lucatello). The observation log is listed in Table 1. The first and last spectra have been obtained in the framework of other UVES programmes (such as the ESO Large Programme on "First Stars"; e.g., Spite et al. 2006), and the corresponding radial velocities have been kindly communicated to us by M. Spite and J. Johnson. The two spectra exposed for 3600 s on the blue arm of UVES (two times 1800 s on the red arm) were used to derive the abundances (Sect. 6). Their signal-to-noise (SNR) ratio is around 200/1 at 400 nm. The spectra exposed for 90 s were only used to derive radial velocities by cross-correlating the observed spectrum with the two high-SNR spectra. The adopted heliocentric velocity for a given low-SNR spectrum is the average of these two differential values; it is listed in Table 1. Arcturus and solar templates were used to estimate the internal consistency of the radial-velocity measurement, and a telluric template spectrum was used to evaluate the zero point offset velocity. The uncertainty on the radial velocity is the root mean square of the template error and the precision of the centering of the Gaussian fit to the cross-correlation profile. Both uncertainty sources, along with their root mean square error, are listed in Table 1.

The standard deviation of the observed radial velocities amounts to 1.24 km s^{-1}, which is considerably larger than the average uncertainty, amounting to only 0.18 km s^{-1}. Possible causes for these variations are investigated in Sect. 4.2.

Table 2. Available photometry for CS 30322-023; m and m_0 are the observed and de-reddened magnitudes in the considered band, respectively.

Band	m	±	m_0	Ref.
U	14.48	0.02	14.19	(1)
B	13.49	0.03	13.24	(1)
V	12.21	0.03	12.02	(1)
J	10.050	0.024	10.00	(2)
H	9.479	0.024	9.45	(2)
K	9.313	0.021	9.30	(2)
Bol.			11.7	(3)

(1) Norris et al. (1999); (2) Cutri et al. (2003); (3) this work.

Broadband UBV photometry is provided by Norris et al. (1999), while near-infrared JHK photometry is available from the *Two Micron All Sky Survey* (Cutri et al. 2003), as listed in Table 2. Given the large distance to CS 30322-023 (Sect. 4), the reddening along its line of sight across the Galaxy was taken from Burstein & Heiles (1982) to be $E_{B-V} = 0.06$, from which it follows that $A_{\rm V} = 0.18$ mag. This value is close to the 0.16 mag predicted by the model of Arenou et al. (1992). The reddening law $A_\lambda/A_{\rm V}$ from Cohen et al. (1981), appropriate for carbon stars, has been applied to deredden the observed magnitudes. Zero-magnitude fluxes from Schmidt-Kaler (1982) and Cohen et al. (2003b) have been used to construct the spectral energy distribution. The bolometric flux has then been obtained by computing the integral $\int \lambda F_\lambda \, {\rm d} \ln \lambda$ using the trapezoidal rule on the UBV and JHK bands. A bolometric correction of -0.30 mag is finally obtained, yielding $m_{\rm bol} = 11.7$. It should be noted that this bolometric correction differs somewhat from the value

Table 3. Atmospheric parameters of CS 30322-023. In the third column, "PP" stands for plane-parallel and "S" for spherical (see text for a discussion of the uncertainties).

$T_{\rm eff}$ (K)	4100	excitation balance (PP-model)
	4100	excitation balance (S-model)
	4350	2MASS photometry
$\log g$	-0.3 ± 0.3	Fe I/Fe II ionisation balance in PP-model (LTE)
	<-0.3	Fe I/Fe II ionisation balance in S-model (LTE)
microturbulent vel. (km s^{-1})	2.2	PP-model
	1.7	S-model

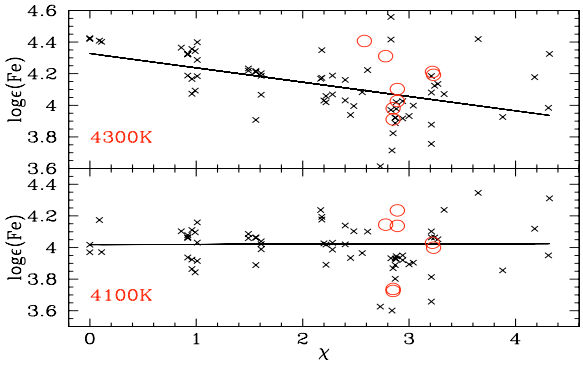

Fig. 1. Iron abundances derived from all lines measured in CS 30322-023 (crosses: Fe I lines; open circles: Fe II lines), as a function of the lower excitation potential for the adopted model (*Lower panel*: $T_{\rm eff}$ = 4100 K, $\log g = -0.3$) and for a model of higher temperature and gravity (*Upper panel*: $T_{\rm eff}$ = 4300 K, $\log g$ = 0.5). The latter model – the best one at 4300 K – is seen to be less satisfactory than the adopted 4100 K model. In both cases, plane-parallel LTE model atmospheres (with [Fe/H] = −3.5 and a microturbulent velocity of 2.2 km s^{-1}) have been used.

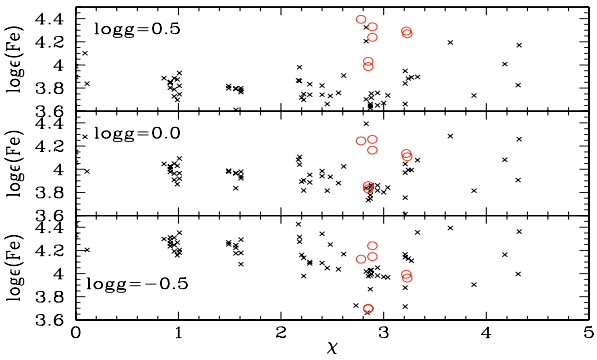

Fig. 2. Same as Fig. 1 for different gravities at $T_{\rm eff}$ = 4100 K.

of −0.8 mag predicted by Table 6 of Alonso et al. (1999) for giants with [Fe/H] = −3 and $T_{\rm eff}$ = 4100 K.

3. Atmospheric parameters of CS 30322-023

The effective temperature of CS 30322-023 was obtained, in the usual manner, by requiring that the abundances derived from various iron lines exhibit no trend with excitation potential. Gravity was obtained through ionisation balance, and microturbulence was set by requiring the absence of a trend between abundances and reduced equivalent widths. A photometric $T_{\rm eff}$ estimate has been obtained from the calibration of Alonso et al. (1998), applied on the 2MASS $J-H$ and $J-K$ indices, assuming a metallicity of −3.0.

The derived atmospheric parameters, using model atmospheres belonging to the OSMARCS family (Gustafsson et al. 2003), are listed in Table 3. The discrepancy between the photometric and spectroscopic temperature estimates probably results, on one hand, from the fact that the CS 30322-023 parameters fall at the edge of the validity domain of Alonso's calibration and, on the other hand, from model errors impacting the spectroscopic determination, as we now discuss. Figure 1 reveals that a temperature $T_{\rm eff}$ = 4300 K, as suggested by the photometric calibration, combined with a higher gravity, does not yield a satisfactory solution. Figure 2, which presents the Fe I and Fe II abundances derived from various lines for plane-parallel, LTE model atmospheres, shows that the best solution is obtained for $T_{\rm eff}$ = 4100 K and $\log g = -0.3$. The uncertainty on the gravity, in the framework of Fe I/Fe II ionisation equilibrium under LTE (see, however, the dicussion about NLTE effects below), may be estimated by comparing the three panels of Fig. 2, corresponding to $\log g$ = 0.5, 0.0 and −0.5. The gravity of CS 30322-023 clearly lies between −0.5 and 0.0. The value $\log g = -0.3 \pm 0.3$ has therefore been adopted.

We have also attempted to employ spherical atmosphere models, which are better suited to low-gravity stars than the conventionally used plane-parallel models. The Fe I/Fe II ionisation balance would require spherical models with an effective gravity $\log g < -0.3$. We could not, however, converge models with such low surface gravities, due to the combination of the large atmospheric extension and the scattering character of the radiation field at such low metallicities, which is decoupled from the local thermal pool of the gas.

It should be noted that the gravities of metal-poor giants derived from LTE iron-line analyses are most probably underestimated, because of the neglect of non-LTE effects (Thévenin & Idiart 1999; Israelian et al. 2001, 2004; Korn et al. 2003). We plan to investigate these effects in a forthcoming paper with models specifically tailored to CS 30322-023. Nevertheless, the conclusion that CS 30322-023 is the most evolved star found thus far among CEMP stars remains valid, as the comparison presented in Fig. 3 involves stars analyzed under LTE as well. In absolute terms, with NLTE corrections on the gravity of 0.5 dex (as derived by Thévenin & Idiart 1999; Korn et al. 2003, for giant stars with [Fe/H] = −3) or even up to 1.0 dex (from the comparison of LTE and NLTE gravities for CS 29498-043 derived by Aoki et al. 2002d; Israelian et al. 2004), CS 30322-023 would remain on the TP-AGB (Figs. 3 and 4).

4. Evolutionary status of CS 30322-023

4.1. Position in the Hertzsprung-Russell diagram

The gravity and effective temperatures derived in Sect. 3 may be combined with the apparent bolometric magnitude to derive the distance of CS 30322-023 as a function of the adopted mass,

Table 4. Distance of CS 30322-023 as a function of the adopted mass, assuming $\log g = -0.3$, $T_{\rm eff} = 4100$ K and $m_{\rm bol} = 11.7$ (corresponding to $BC_V = -0.3$ and $A_V = 0.18$ mag). Solutions corresponding to this set of parameters are listed under the header "set (1)", whereas an alternative solution, accounting for uncertainties in gravity and temperature, is listed under the header "set (2)" ($\log g = 0.7$, $T_{\rm eff} = 4350$ K and $m_{\rm bol} = 11.7$). The ages up to the TP-AGB phase are read from Fig. 8 for the 0.8, 4, and 9 $M_\odot$ models.

$M/M_\odot$	set	$\log L/L_\odot$ (1)	$\log L/L_\odot$ (2)	$M_{\rm bol}$ (1)	$M_{\rm bol}$ (2)	d (kpc) (1)	d (kpc) (2)	age (y)
10		5.15	4.24	−8.1	−5.9	92	33	–
9		5.10	4.20	−8.0	−5.8	87	31	2.5×10^7
5		4.84	3.94	−7.4	−5.1	65	23	–
4		4.75	3.85	−7.1	−4.9	58	21	1.6×10^8
3		4.62	3.72	−6.8	−4.6	50	18	–
1		4.15	3.24	−5.6	−3.4	29	10	–
0.8		4.05	3.14	−5.4	−3.1	26	9	13.8×10^9

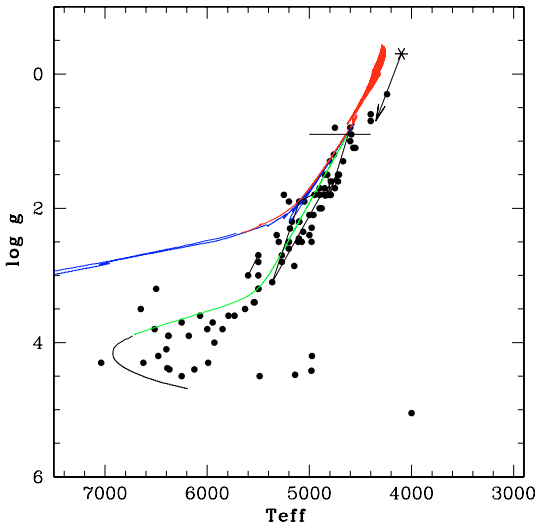

Fig. 3. Hertzsprung-Russell diagram for CEMP stars collected from the literature (see references in the text), revealing that CS 30322-023 (asterisk) is the most extreme case known. The solid line corresponds to the evolutionary track of a 0.8 $M_\odot$ model with [Fe/H] = −3.8 (see text). The horizontal bar on the evolutionary track marks the tip of the RGB. The arrow corresponds to a conservative 250 K uncertainty on $T_{\rm eff}$ and a 1.0 dex uncertainty on the gravity of CS 30322-023 due to the use of LTE instead of NLTE model atmospheres (see text).

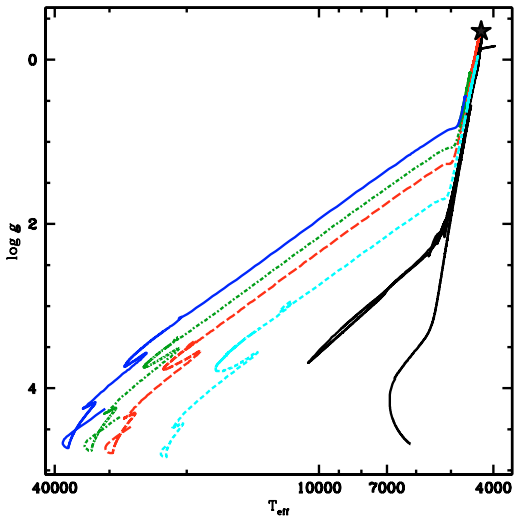

Fig. 4. Evolutionary tracks (in a $\log g - T_{\rm eff}$ plane) of a 0.8 $M_\odot$ model at [Fe/H] = −3.8 (black solid line) and of a 4 $M_\odot$ (cyan short-dashed line), 7 $M_\odot$ (red long-dashed line), 9 $M_\odot$ (green dot-dashed), and 12 $M_\odot$ (blue solid line), at metallicity $Z = 10^{-5}$ ([Fe/H] $\simeq -3.3$), computed with STAREVOL (Siess 2006) from the main sequence to the thermally-pulsing AGB phase (for the 0.8, 4, 7 and 9 $M_\odot$ models), and to neon ignition for the 12 $M_\odot$ model. The position of CS 30322-023 is represented by the asterisk.

using the relationship:

$$\log M/M_\odot = \log g/g_\odot + \log L/L_\odot - 4 \log T_{\rm eff}/T_{\rm eff,\odot} \quad (1)$$
$$= -2.25 - 0.4 M_{\rm bol} \quad (2)$$
$$= 2 \log d\,({\rm pc}) - 8.93, \quad (3)$$

where we have adopted $T_{\rm eff} = 4100$ K, $\log g = -0.3$ and $m_{\rm bol} = 11.7$ for CS 30322-023 (denoted set (1) in Table 4). The corresponding distances and luminosities are listed in Table 4. To illustrate the effects of the uncertainties, values for $\log L/L_\odot$, $M_{\rm bol}$ and d (listed under set (2)) have been derived assuming that the gravity could be 1 dex higher (due to NLTE effects) and the temperature 250 K higher.

CS 30322-023 appears to be the star with the lowest gravity detected so far among CEMP stars, as shown in Fig. 3, which collects all such stars from the literature (Dearborn et al. 1986; Ryan et al. 1991; McWilliam et al. 1995; Norris et al. 1997a,b; Sneden et al. 1998; Gratton et al. 2000; Hill et al. 2000; Sneden et al. 2000; Westin et al. 2000; Norris et al. 2001; Preston & Sneden 2001; Van Eck et al. 2001; Travaglio et al. 2001; Aoki et al. 2001; Christlieb et al. 2002; Hill et al. 2002; Johnson & Bolte 2002; Aoki et al. 2002a,b,c,d, 2003; Cohen et al. 2003a; Lucatello et al. 2003; Sneden et al. 2003; Van Eck et al. 2003; Aoki et al. 2004; Cohen et al. 2004; Honda et al. 2004; Johnson & Bolte 2004; Simmerer et al. 2004; Barbuy et al. 2005; Plez & Cohen 2005; Frebel et al. 2005, 2006; Masseron et al. 2006).

With $T_{\rm eff} = 4240$ K and $\log g = 0.3$, the star HD 110184 (which, despite the reported detection of Th, is not considered an r-process enhanced star, according to the criteria of Beers & Christlieb 2005; its [Eu/Fe] ratio is too low) studied by Honda et al. (2004) is the second most evolved star after CS 30322-023. Then comes CS 29498-043, studied by Aoki et al. (2002d, 2004), Weiss et al. (2004), and Israelian et al. (2004), with $T_{\rm eff} = 4400$ K and $\log g = 0.6$ (Aoki et al. 2002d, a subsequent analysis by Aoki et al. 2004, yielded instead $T_{\rm eff} = 4600$ K and $\log g = 1.2$). Using a NLTE analysis on Fe lines, Israelian et al. (2004) derive a higher gravity ($\log g = 1.5$), thus indicating that LTE analyses underestimate the gravity by about 1 dex for this star.

Stars that may also be located above the tip of the red-giant branch (predicted to occur at $\log g = 0.9$ in a 0.8 $M_\odot$, [Fe/H] = −3.8 model, as indicated by the horizontal mark on the evolutionary track of Fig. 3) also include CS 30314-067 (Aoki et al. 2002c), CS 22948-027 (Preston & Sneden 2001, but here

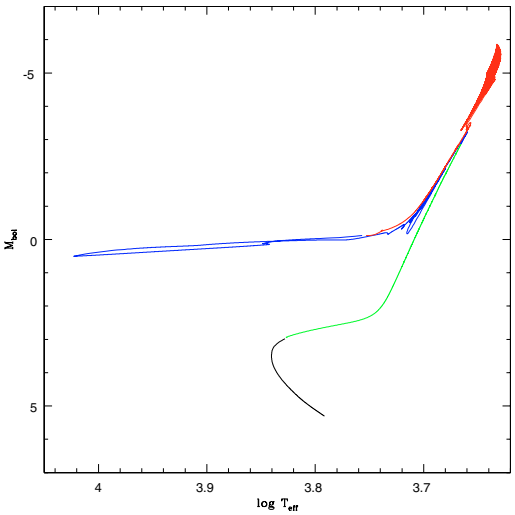

Fig. 5. Same as Fig. 4 for the 0.8 $M_\odot$ model in the usual $M_{\rm bol} - T_{\rm eff}$ plane.

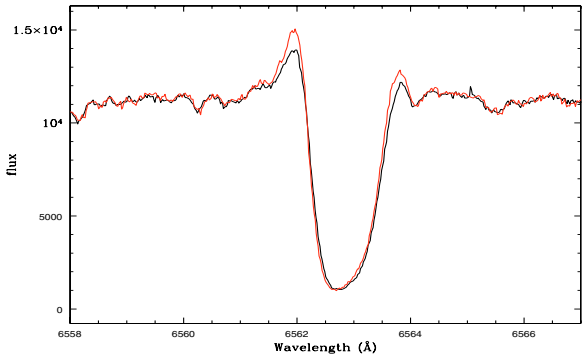

Fig. 6. Sample spectra around the Hα line (the flux is in arbitrary units), obtained on 2002/04/24 and 2002/05/11. The change in the profile over 17 days reflects some kind of activity, such as, for instance, a strong wind.

again Barbuy et al. 2005, obtain a larger $\log g$ value of 1.8), and CS 30301-015 (Aoki et al. 2002d).

Mauron et al. (2004, 2005) list about 120 cool carbon stars in the halo (with *JHK* colors very similar to those of CS 30322-023), located at quite large galactocentric distances (up to 120 kpc!). They were not plotted in Fig. 3, however, as neither their metallicities nor their gravities are known.

The low gravity derived for CS 30322-023 appears, at first sight, quite puzzling. A comparison with low-metallicity stellar evolution tracks reveals, however, that both the gravity and effective temperature of CS 30322-023 are in fact typical of low-metallicity red-giant stars. Figure 4 displays the evolutionary tracks in a gravity – effective temperature plane for a 0.8 $M_\odot$ model of metallicity [Fe/H] = −3.8, and for intermediate-mass stars of 4, 7, 9 and 12 $M_\odot$ and $Z = 10^{-5}$ ([Fe/H] = −3.3), computed with STAREVOL (Siess 2006) all the way from the pre-main sequence to the thermally-pulsing AGB stage (for the 0.8, 4, 7 and 9 $M_\odot$ models), and to the ignition of neon for the 12 $M_\odot$ model. For these computations, we use the Reimers (1975) mass-loss rate up to the end of core He burning, and then switch to the Vassiliadis & Wood (1993) prescription during the AGB phase. The region around $\log g = 0$ and $\log T_{\rm eff} = 3.61$ is reached by all five models, thus providing a non-unique solution! However, each of these possible solutions presents its own difficulties. In the case of the 0.8 $M_\odot$ model, the evolutionary timescales may be a problem. Although the model star has a total lifetime of 13.8 Gyr (about the age of the Galaxy), the time spent by such stars in the TP-AGB phase might seem prohibitively short to ensure that some are actually observed. We will show in Sect. 5 that this is not the case, since the short time span on the TP-AGB is more than offset by the large volume within which these very luminous stars may be detected. In the case of the intermediate or massive stars, one may wonder whether such massive short-lived stars could still be found in the galactic halo, especially since the distance estimates for CS 30322-023 presented in Table 4 places it at the outskirts of the halo.

4.2. Observational evidence

The variability observed for the Hα line profile suggests the presence of a stellar wind (Fig. 6), and provides a further argument in favour of the very evolved nature of CS 30322-023.

Unfortunately, there is no available information on possible optical variability, which should be present if CS 30322-023 lies high on the AGB. The profile resulting from the correlation of the spectrum with the Arcturus template used to derive the radial velocity also does not exhibit the asymmetric shape expected for Mira variables experiencing shock waves in their photospheres (Alvarez et al. 2001). Nonetheless, as we now show, the available radial-velocity data (Table 1) exhibit properties that appear to be typical of low-metallicity pulsating stars.

It was shown in Sect. 2 that the radial velocity standard deviation (1.24 km s^{-1}) is considerably larger than the average uncertainty, amounting to 0.18 km s^{-1}. These variations may be caused either by the pulsation of the stellar envelope or by an orbital motion in the presence of a companion (or a combination of both). Let us first stress that the stellar properties listed in Table 4 put stringent constraints on the admissible orbital periods. For an 0.8 $M_\odot$ star, the stellar radius corresponds to 210 $R_\odot$ with atmospheric parameter set (1) (i.e., $T_{\rm eff} = 4100$ K and $\log g = -0.3$), and to 65 $R_\odot$ for set (2) (i.e., $T_{\rm eff} = 4350$ K and $\log g = 0.7$). In a binary system involving two stars of 0.8 $M_\odot$ (the primary being the observed low-metallicity star assumed to be a long-lived low-mass star and the secondary a white dwarf), the minimum admissible orbital periods corresponding to CS 30322-023 not filling its Roche lobe amount to 1180 d and 200 d, respectively. These periods represent absolute lower limits, since higher-mass stars have larger radii, and hence longer threshold orbital periods.

Interestingly, a sine-wave of period 192 d very nicely fits the radial-velocity data at JD > 2 453 000 (upper panel of Fig. 7). From the above considerations, this signal has too short a period to represent an orbital motion; moreover, it does not fit the earlier data points. It is likely, therefore, that it represents pulsation of the stellar envelope. The pulsation periods of low-metallicity stars are shorter than those of solar-metallicity Miras, and their range matches the 192 d period observed for CS 30322-023 (Alvarez et al. 1997). The poor fit to the earlier data points may either be caused by a sudden phase shift of the (possibly semi-regular) pulsation, or by a long-term trend associated with a binary motion.

We now consider the latter possibility. The dashed line in the lower panel of Fig. 7 corresponds to a shift of 1.0 km s^{-1} over 1000 d. It provides a better fit to the earlier data points; such a trend is not unexpected for binary systems involving chemically-peculiar red giants such as CS 30322-023. To fix the ideas, let us assume that CS 30322-023 is a binary with a period of 5200 d, as is typical for barium stars (Jorissen 2003). In this case, our measurements have only sampled a quarter of the orbital cycle.

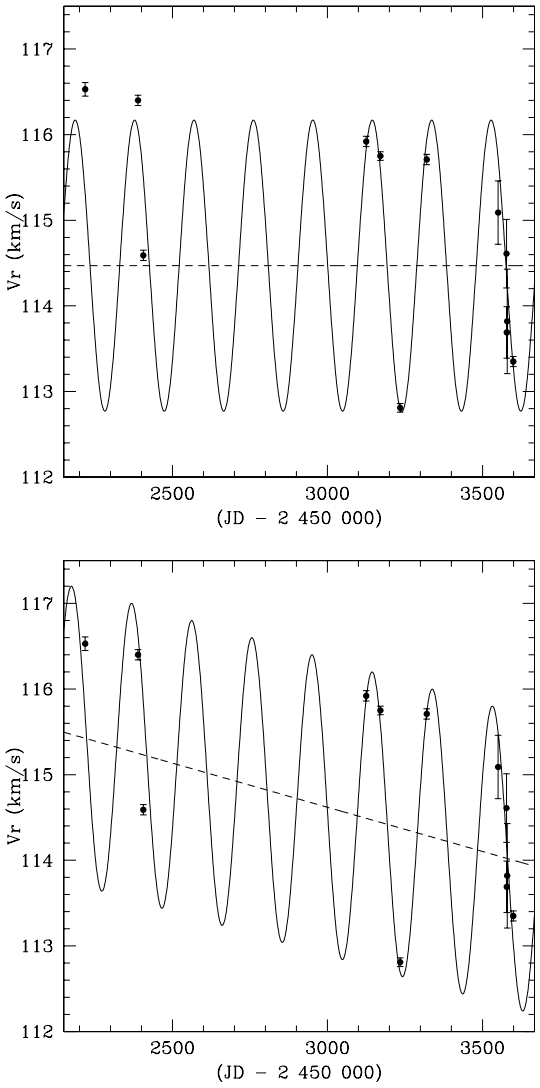

Fig. 7. Radial velocity as a function of Julian date. *Top panel*: a sine-wave of period 191.7 d, fitted on the data points with JD > 2 453 000. *Lower panel*: the same sine-wave superimposed on a linear trend of 1.0 km s^{-1} per 1000 d, possibly representing an orbital motion.

In the most favourable case, the observed velocity range is then equal to the velocity semi-amplitude, K, which would amount to 7.2 km s^{-1} for a circular orbit seen edge-on and involving two stars of 0.8 $M_\odot$ (see above). The possible long-term trend of 1.3 km s^{-1} over 1300 d is not incompatible with the above estimate of K, provided that the orbital plane is inclined on the sky.

To conclude this discussion, there is no firm support in favour of the binary nature of CS 30322-023, although in this case the absence of evidence is not evidence of absence, especially since any orbital motion will be very difficult to disentangle from the large intrinsic jitter. The binary hypothesis will therefore be left open in the discussion of Sect. 7.

5. Probability of observing an extremely metal-poor TP-AGB star

Since it is very unlikely that a massive or intermediate-mass star has been formed in a recent star-forming episode at such large galactocentric distances (>20 kpc, Table 4) in the halo of the Galaxy, in this section we evaluate the likelihood of an alternative scenario, that CS 30322-023 is a TP-AGB star formed shortly after the birth of the Galaxy.

We now estimate the relative fraction of halo TP-AGB stars in a magnitude-limited sample (such as the HK survey), as compared to main-sequence turnoff or horizontal-branch stars *from a co-eval sample*. The assumption of co-evality is probably valid as long as one restricts the sample to extremely metal-poor stars with [Fe/H] < −3.0. We further assume that a star of 0.8 $M_\odot$ with [Fe/H] = −3.8 has a lifetime (up to the planetary nebula phase) precisely equal to the age of the galactic halo (Sect. 4)[1].

In an ideal co-eval sample (i.e., not subject to observational selection biases) consisting of the oldest stars in the Galaxy with $M \geq M_{\rm low}$, $M_{\rm low}$ being the low-mass cutoff of the population (to be fixed below), the fraction, F, of TP-AGB stars expected in such a sample is:

$$F = \frac{\int_{M_{\rm AGB}}^{0.8\,M_\odot} \Psi_{\rm IMF}(M)\,{\rm d}M}{\int_{M_{\rm low}}^{0.8\,M_\odot} \Psi_{\rm IMF}(M)\,{\rm d}M}, \quad (4)$$

where $\Psi_{\rm IMF}$ is the initial mass function. Here we adopt $\Psi_{\rm IMF}(M) \propto M^{-1.3}$ for the mass range [0.1, 0.5] $M_\odot$, and $\Psi_{\rm IMF}(M) \propto M^{-2.3}$ for the mass range]0.5, 0.8] $M_\odot$ (Kroupa 2001). In Eq. (4), $M_{\rm AGB}$ corresponds to the mass of a halo star currently entering the TP-AGB phase. Before the TP-AGB phase, the star will have gone successively through the main-sequence, the main sequence turn-off (TO), the red-giant-branch phase (RGB), the core helium-burning or horizontal-branch phase (HB), and the early-AGB phase, the latter two being considered as a whole in what follows. Similarly to $M_{\rm AGB}$, one may define the threshold masses $M_{\rm TO}$, $M_{\rm RGB}$, and $M_{\rm HB}$ for stars formed at the birth of the Galaxy and currently entering these various evolutionary phases. These masses may be defined from evolutionary time-scale considerations, since all of these stars are supposed to be co-eval with the age of the Galaxy $\tau_{\rm Galaxy}$. Hence,

$$\begin{aligned}
\tau_{\rm Galaxy} &= \tau_{\rm MS}(0.8) + \tau_{\rm TO}(0.8) + \tau_{\rm RGB}(0.8) \\
&\quad + \tau_{\rm HB}(0.8) + \tau_{\rm AGB}(0.8) \\
&= \tau_{\rm MS}(M_{\rm AGB}) + \tau_{\rm TO}(M_{\rm AGB}) + \tau_{\rm RGB}(M_{\rm AGB}) \\
&\quad + \tau_{\rm HB}(M_{\rm AGB}) \\
&= \tau_{\rm MS}(M_{\rm HB}) + \tau_{\rm TO}(M_{\rm HB}) + \tau_{\rm RGB}(M_{\rm HB}) \\
&= \tau_{\rm MS}(M_{\rm RGB}) + \tau_{\rm TO}(M_{\rm RGB}) \\
&= \tau_{\rm MS}(M_{\rm TO}).
\end{aligned}$$

The last equation of the above set indicates that the stars now at the main-sequence TO have a mass $M_{\rm TO}$, so that their lifetime on the main sequence equals the age of the Galaxy. The mass, $M_{\rm RGB}$, of stars now entering the red-giant-branch stage is then given by combining the last two equations in the above set:

$$\tau_{\rm MS}(M_{\rm TO}) - \tau_{\rm MS}(M_{\rm RGB}) = \tau_{\rm TO}(M_{\rm RGB}), \quad (5)$$

or, in other words, the difference $\delta\tau_{\rm MS}(M_{\rm RGB})$ of the main-sequence lifetimes of the stars of masses $M_{\rm TO}$ and $M_{\rm RGB}$ is just equal to the time spent on the TO by the star of mass $M_{\rm RGB}$ currently entering the RGB. This difference, $\delta\tau_{\rm MS}(M_{\rm RGB})$, relates to the mass difference, $\delta M = M_{\rm TO} - M_{\rm RGB}$, through the lifetime, $\tau_{\rm MS}$, of main-sequence stars:

$$\tau_{\rm MS} \propto M^{-2.5}, \quad (6)$$

[1] We assume in this section that the lifetimes derived from the stellar models with [Fe/H] = −3.8 apply to CS 30322-023, despite the small difference in metallicity.

leading to

$$\frac{\delta\tau_{\rm MS}}{\tau_{\rm MS}} = -2.5\ \frac{\delta M}{M}. \quad (7)$$

Solving for $M_{\rm RGB}$ then yields:

$$M_{\rm RGB} = M_{\rm TO}\left(1 + 0.4\ \frac{\tau_{\rm TO}(M_{\rm RGB})}{\tau_{\rm MS}(M_{\rm TO})}\right). \quad (8)$$

The other masses are derived in a similar way:

$$M_{\rm HB} = M_{\rm TO}\left(1 + 0.4\frac{\tau_{\rm TO}(M_{\rm HB})}{\tau_{\rm MS}(M_{\rm TO})} + 0.4\frac{\tau_{\rm RGB}(M_{\rm HB})}{\tau_{\rm MS}(M_{\rm TO})}\right)$$

$$M_{\rm AGB} = M_{\rm TO}\left(1 + 0.4\frac{\tau_{\rm TO}(M_{\rm AGB})}{\tau_{\rm MS}(M_{\rm TO})} + 0.4\frac{\tau_{\rm RGB}(M_{\rm AGB})}{\tau_{\rm MS}(M_{\rm TO})} + 0.4\frac{\tau_{\rm HB}(M_{\rm AGB})}{\tau_{\rm MS}(M_{\rm TO})}\right)$$

$$0.8 = M_{\rm TO}\left(1 + 0.4\frac{\tau_{\rm TO}(0.8)}{\tau_{\rm MS}(M_{\rm TO})} + 0.4\frac{\tau_{\rm RGB}(0.8)}{\tau_{\rm MS}(M_{\rm TO})} + 0.4\frac{\tau_{\rm HB}(0.8)}{\tau_{\rm MS}(M_{\rm TO})} + 0.4\frac{\tau_{\rm AGB}(0.8)}{\tau_{\rm MS}(M_{\rm TO})}\right).$$

The last equation above is used to derive $M_{\rm TO}$. An iterative procedure is required, since the lifetime ratios must be normalized by the main-sequence lifetime of a star of yet-unknown mass, $M_{\rm TO}$. In the first iteration, the various lifetime ratios *normalized by the main-sequence lifetime of the 0.8 $M_\odot$* star (namely 12.2×10^9 y, up to the turn-off at $M_{\rm bol} \sim 3.5$) are read from Fig. 9, namely $\tau_{\rm HB}(0.8)/\tau_{\rm MS}(0.8) = 0.006$, $\tau_{\rm RGB}(0.8)/\tau_{\rm MS}(0.8) = 0.045$, and $\tau_{\rm TO}(0.8)/\tau_{\rm MS}(0.8) = 0.08$.

The lifetime spent on the TP-AGB, $\tau_{\rm AGB}$, is very sensitive to the adopted mass-loss rate prescription. Very little is known about mass loss in extremely low-metallicity stars (van Loon 2006). If it is driven by radiation pressure, then stellar wind models (Kudritzki et al. 1987, 1991; van Loon 2000) indicate that the rate depends roughly on the square root of the metallicity. Observational support for the sensitivity of mass-loss rate to metallicity has been provided by Groenewegen et al. (1995), who compare the dust content of LMC and galactic AGB stars of similar pulsational periods. Alternatively, Vassiliadis & Wood (1993) derived an empirical formulation of the mass-loss rate based on the pulsational properties of the Mira variables and pulsating OH/IR stars. Their expression is not explicitly dependent on metallicity, but it does include the effect of the chemical composition through the stellar parameters entering the computation of the pulsational period. When the mass-loss rate depends upon metallicity, it remains quite low (and hence the AGB lifetime quite long) unless third dredge-up (3DUP) episodes increase the metal content of the envelope and boost the mass-loss rate. This prescription implies a longer lifetime on the TP-AGB than the Vassiliadis & Wood prescription. Therefore, the TP-AGB lifetime displayed in Figs. 8 and 9, computed with the Vassiliadis & Wood prescription, is likely to represent a lower limit on the actual lifetime. Moreover, in our calculations, only 26 pulses have taken place, and the envelope mass still amounts to 0.1 $M_\odot$ with a mass loss rate of 4×10^{-8} $M_\odot$ y^{-1}. The TP-AGB lifetime displayed in Fig. 8 for the 0.8 $M_\odot$ model therefore represents a lower bound to the actual lifetime, which may be expected to be longer by a few 10^6 y.

Given the uncertainty affecting $\tau_{\rm AGB}$, it will be kept as a free parameter for the remainder of this section. Nevertheless, as an illustrative example, conservatively adopting $\tau_{\rm AGB}(0.8) = 10^7$ y yields $\tau_{\rm AGB}(0.8)/\tau_{\rm MS}(0.8) = 8\times10^{-4}$, hence $\tilde{M}_{\rm TO} = 0.760\ M_\odot$. From Eq. (7), such a star has a main-sequence lifetime 1.5×10^9 y longer than the 0.8 $M_\odot$ one, or $\tau_{\rm MS}(M_{\rm TO})/\tau_{\rm MS}(0.8) = 1.12$. This factor is thus applied to the above lifetime ratios to normalize them by $\tau_{\rm MS}(M_{\rm TO})$, as required. The adopted ratios are listed in Table 5. This second (and last) iteration then yields

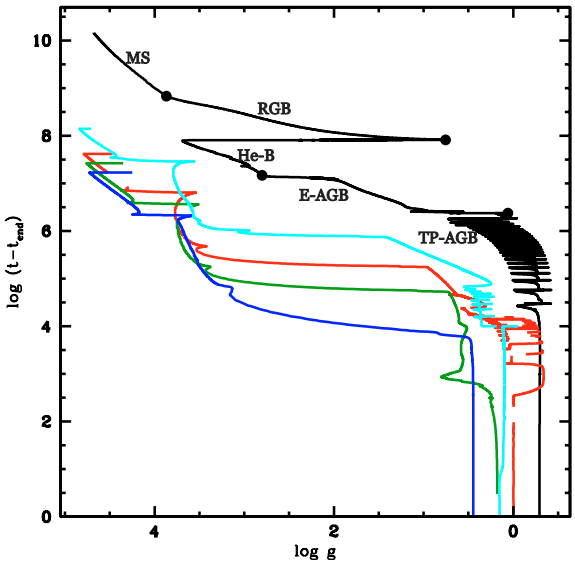

Fig. 8. Same as Fig. 4 for the ages of the five models as a function of the effective gravity. The age is counted backward from the last computed model. The occurrence of thermal pulses is evident from the rapid oscillations of log g near the end of the evolution. The large dots on the 0.8 $M_\odot$ track mark the transition between different evolutionary phases: main sequence (labelled MS), red giant branch (RGB), core helium-burning (He-B), early AGB (E-AGB), and thermally-pulsing AGB (TP-AGB).

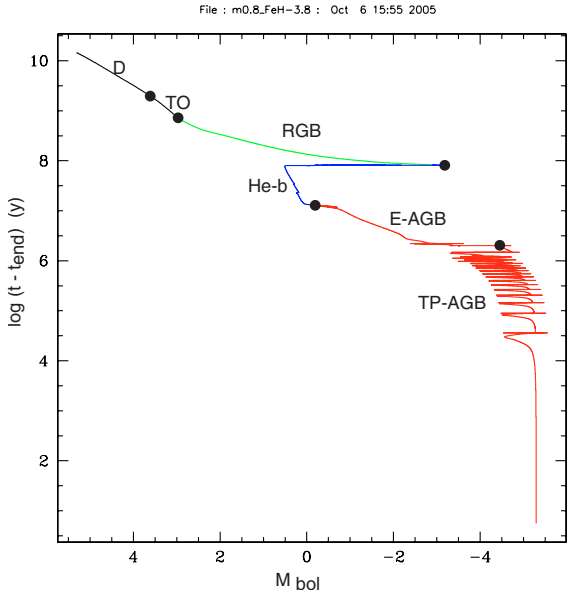

Fig. 9. Same as Fig. 8 for the 0.8 $M_\odot$ model, but expressed as a function of $M_{\rm bol}$. The lifetimes in the different evolutionary stages are used in Sect. 5. Note that the AGB lifetime provided by this figure is a lower limit to the actual value, since only 26 pulses have been computed, and the remaining envelope mass amounts to 0.1 $M_\odot$. A few million years should thus be added to the AGB lifetime displayed on the figure. Moreover, the Vassiliadis & Wood (1993) prescription for the mass loss used in these computations (see text) also shortens the AGB lifetime.

Table 5. Sampling distances of the HK survey for the various stellar subtypes and fractional lifetimes $\tau(0.8)/\tau_{\rm MS}(M_{\rm TO})$ for the various evolutionary phases of the 0.8 $M_\odot$ model of [Fe/H] = −3.8. The lifetime in the AGB phase is subject to various uncertainties, and has therefore not been listed. BC_B and A_B are, respectively, the bolometric correction and total absorption in the B band.

type i	$\tau_i(0.8)/\tau_{\rm MS}(M_{\rm TO})$	$\log T_{\rm eff}$	$M_{\rm bol}$	BC_B	A_B	$d_{\rm min}$ (kpc)	$d_{\rm max}$ (kpc)	$n_{\rm vol}/n_{\rm vol,TO}$
AGB	–	3.61	−5	−1.6	0.2	6.91	69.1	274
HB + E-AGB	5.6×10^{-3}	3.85	0.5	−0.5	0.2	0.91	9.12	40.8
RGB	4.0×10^{-2}	3.71	0.5	−1.0	0.2	0.72	7.24	24.7
TO	6.9×10^{-2}	3.85	3.5	−0.5	0.0	0.25	2.51	1
MS	0.88	3.81	5	−0.5	0.0	0.12	1.23	–

$M_{\rm TO} = 0.764\ M_\odot$. Since all five threshold masses are very close to one another, the normalized lifetimes appearing in the equation set above will all be taken equal to the values corresponding to the 0.8 $M_\odot$ model listed in Table 5.

To describe a real stellar sample (which in this case is magnitude limited), the observational censorship needs to be included, implying that the sampling volume will depend on the luminosity of the various classes of stars, thus largely favouring bright stars, such as AGB stars, over main-sequence stars. In the following, the integral appearing in the denominator of Eq. (4) will be split into five different components – thermally-pulsing AGB (TP-AGB) stars, horizontal-branch and early AGB stars (collectively referred to as HB), main-sequence turnoff stars (TO), and finally main-sequence stars (MS). The lower limit of the main-sequence mass range considered in Eq. (4) is denoted $M_{\rm low}$; however, as shown below, it has no significant impact on the final result.

With these conventions, Eq. (4) can be rewritten

$$P_{\rm AGB} = \frac{n_{\rm vol_{AGB}} \int_{M_{\rm AGB}}^{0.8\,M_\odot} \Psi_{\rm IMF}(M)\ {\rm d}M}{\Sigma_{i=1}^{5} n_{{\rm vol},i} \int_{M_i}^{M_{i+1}} \Psi_{\rm IMF}(M)\ {\rm d}M}, \quad (9)$$

where $n_{\rm vol}$ is the number of halo stars in the volume sampled for the various subtypes of stars (namely TP-AGB, HB, RGB, TO, and MS; $M_1 = M_{\rm low}, M_2 = M_{\rm TO}$..., $M_6 = 0.8\ M_\odot$), given the fact that the HK sample is limited to the $11 \le B \le 16$ magnitude range (Beers et al. 1992). The adopted volume is a cone along the line of sight to CS 30322-023, truncated at a minimum distance fixed by $B = 11$, and the absolute B magnitude of the considered stellar subtype, and at a maximum distance similarly fixed by the condition $B = 16$. The halo star number density is assumed to decrease as $[R^2 + (z/0.76)^2]^{-2.44/2}$, R being the galactocentric distance measured in the galactic plane and z the distance from the plane, according to the model of Robin et al. (2003).

The distance cut-offs, $d_{\rm min,max}$, for the RGB, HB, and AGB stars are listed in Table 5, along with the adopted bolometric magnitudes and effective temperatures (from the STAREVOL tracks discussed in Sect. 4 and displayed in Fig. 5), bolometric corrections and total galactic absorption in the B band along the line of sight to CS 30322-023, according to the discussion in Sect. 3. For TO and MS stars, galactic absorption is assumed to be negligible, since the volume sampled is small. The bolometric correction in the B band is taken from a grid of MARCS models with [Fe/H] = −4, and a range of gravities and effective temperatures. They do not differ much from those provided in Table 6 of Alonso et al. (1999) for giants with [Fe/H] = −3. The bolometric correction for AGB stars has been taken identical to that derived for CS 30322-023 (Sect. 2).

Main-sequence stars are sampled in an exceedingly small volume as compared to the other, more luminous classes, as may be judged from Table 5. Those stars should thus be very rare among the HK survey (Beers et al. 1985) since the volume effect largely offsets the effect of the increasing IMF, hence the first term ($i = 1$) of the sum in Eq. (9) is neglected in the following.

The number of stars in a truncated cone along the line of sight to CS 30322-023, with an opening angle of α (this parameter, appearing in both the numerator and denominator of Eq. (9), has no impact on the final result) thus becomes

$$n_{\rm vol}(M) = \pi\ {\rm tg}^2\alpha\ \rho_0 \int_{d_{\rm min}(M)}^{d_{\rm max}(M)} \left(R^2 + (z/0.76)^2\right)^{-1.22}\ d^2\ {\rm d}\,d \quad (10)$$

where $R = r_0 - d\cos b$ (or $d\cos b - r_0$, whichever is positive) is the galactocentric distance measured in the galactic plane, $z = d\sin b$ the distance from the plane, $b = -46.3°$ is the galactic latitude of CS 30322-023 (its galactic longitude, $l = -6.8°$, is sufficiently close to 0 to be neglected in the above formula), $r_0 \sim 8$ kpc is the galactocentric distance of the Sun, and ρ_0 is the central galactic density of extremely metal-poor halo stars. The latter parameter will later cancel, and thus has no impact on the final result.

The integrals of Eq. (10) have been computed numerically; the results are listed in Table 5. The final proportion of AGB stars in the co-eval sample is displayed in Fig. 10. Given the fact that a reasonable estimate for the fractional TP-AGB lifetime, $\tau_{\rm AGB}(0.8)/\tau_{\rm MS}(M_{\rm TO})$, is on the order of $10^{-3}(=10^7/10^{10}$ y/y), the main conclusion from the present analysis is that it is *not at all unlikely* to observe an extremely low-metallicity TP-AGB star in a co-eval sample. The Beers et al. (1992) sample is most likely not a co-eval sample, as it includes stars with metallicities larger than that of CS 30322-023, which must have formed somewhat more recently. In a sample containing stars formed over a long period of time (with a constant star formation rate), the relative fractions of stars of various kinds are proportional to their lifetimes. Since the lifetime of stars at the main-sequence turnoff is about 70 times longer than the AGB lifetime, it is not surprising that Beers et al. (1992) sample contains a much larger fraction of TO stars than predicted under the co-evality hypothesis. Nevertheless, it should be stressed that the above analysis was not designed to mimick the Beers et al. (1992) sample (this would require a detailed knowledge of the star formation history in the halo, which is beyond the scope of the present paper), but rather to roughly evaluate the likelihood of finding an extremely low-metallicity TP-AGB star. Incidentally, an analysis similar to the one presented here, based on the Bahcall-Soneira Galaxy model (Bahcall & Soneira 1980), was presented by Beers et al. (1985), who arrived at the same conclusion – a magnitude-limited sample of halo stars to apparent magnitude $B = 16$ is, by far, dominated by giant stars.

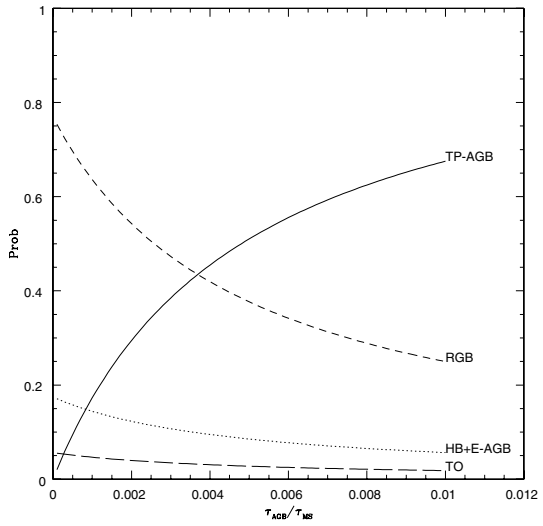

Fig. 10. Fraction of AGB stars (solid line), HB stars (dotted line), RGB stars (short-dashed line), and TO stars (long-dashed line) in a co-eval sample born in the early Galaxy.

6. Abundances

Because of the general crowding of the spectra for cool, evolved stars with molecular lines, the analysis of stars as CS 30322-023 is very challenging. Thanks to the low metallicity, however, abundances could be obtained for 35 species, while seven received upper limits on their abundances with the plane-parallel (PP) model. These results are summarised in Table 6. Hyperfine structure has been included for Ba, La, Pr, Eu, Tb, Dy, Er, Lu, and Pb. C and N abundances are derived from the CH and CN lines. The O abundance is derived from the 630.0 nm [O I] forbidden line which, among the O abundance diagnostics, is expected to be the least affected one by non-LTE conditions (Israelian et al. 2004), although it is sensitive to 3D granulation effects (Shchukina et al. 2005).

Although the gravity has been derived from the Fe I/Fe II ionisation balance, a large discrepancy (about 0.4 dex) is nevertheless found between the abundances derived from the Ti I and Ti II lines. This discrepancy might be ascribed to various causes: (i) the use of a plane-parallel instead of a spherical model (but see the discussion in Sect. 3), (ii) NLTE effects (Thévenin & Idiart 1999; Israelian et al. 2001, 2004; Korn et al. 2003), (iii) 3D effects (Asplund 2005), or (iv) a systematic shift between the scales on which the $\log gf$ values for Ti I and Ti II are derived. A similar problem has been reported for Cr in other cool metal-poor stars (Johnson 2002). The first three possibilities should be investigated in the future by using tailored 3D, NLTE models.

The uncertainty quoted in Table 6 in the column labelled σ does not include such possible systematic errors, as it only refers to the standard deviation of the abundances derived from the different lines used for a given species. When only one line is available, spectrum synthesis has been used, and a 0.1 dex uncertainty should in this case be considered as typical, arising from errors associated with the location of the continuum and on the line-fitting process.

Table 6 reveals that, quite remarkably, the C enhancement in CS 30322-023 is only moderate, in contrast to the N enhancement (Figs. 11 and 12). Na is strongly enhanced as well. The C/O ratio is only 0.50. The C and O abundances are in fact compatible with the trend due to the chemical evolution of the Galaxy, as displayed in Fig. 11 for C and in Fig. 13 for O.

Table 6. Abundances for CS 30322-023 obtained with the plane-parallel model. *N* is the number of lines used in the analysis; "syn" indicates that spectral synthesis has been used to derive the abundance. The column $\log\epsilon$(X) lists the abundance in the scale where $\log\epsilon$(H) = 12. Abundances are normalized by the solar data from Asplund et al. (2005).

Element	*N*	$\log\epsilon$(X)	σ	[X/H]	[X/Fe]
C (CH)	(syn)	5.60	–	–2.79	0.60
N (CN)	(syn)	7.20	–	–0.58	2.81
O I	1(syn)	5.90	–	–2.76	0.63
Na I	4	4.07	0.24	–2.10	1.29
Mg I	4	4.94	0.10	–2.59	0.80
Al I	2	3.70	0.3	–2.67	0.72
Si I	1	4.70	0.2	–2.81	0.58
K I	1(syn)	<3.00	–	–2.08	1.31
Ca I	10	3.37	0.12	–2.94	0.45
Sc II	4	–0.12	0.17	–3.17	0.24
Ti I	10	1.31	0.19	–3.59	–0.20
Ti II	14	1.72	0.13	–3.18	0.23
V II	3(syn)	0.40	0.1	–3.60	–0.19
Cr I	9	1.66	0.22	–3.98	–0.59
Mn I	6	1.66	0.28	–3.73	–0.34
Fe I	66	4.06	0.18	–3.39	0
Fe II	7	4.04	0.19	–3.41	0
Co I	1	1.33	–	–3.59	–0.20
Ni I	6	2.56	0.18	–3.67	–0.28
Cu I	1(syn)	–0.10	–	–4.31	–0.92
Zn I	2	1.23	0.04	–3.37	0.02
Sr II	1(syn)	–1.00	–	–3.92	–0.51
Y II	6	–1.56	0.15	–3.77	–0.36
Zr II	5	–0.68	0.30	–3.27	0.14
Tc I	1(syn)	<–1.40	–	–	–
Ru I	1(syn)	<–0.50	–	–2.34	1.05
Rh I	1(syn)	<–2.00	–	–3.12	0.27
Ba II	3(syn)	–0.70	0.1	–2.87	0.54
La II	8(syn)	–1.80	0.1	–2.93	0.48
Ce II	18	–1.22	0.24	–2.80	0.61
Pr II	3(syn)	–2.50	0.10	–3.21	0.20
Nd II	24	–1.34	0.29	–2.79	0.62
Sm II	4(syn)	–2.30	0.2	–3.31	0.10
Eu II	1(syn)	–3.40	–	–3.92	–0.51
Gd II	1(syn)	<–2.30	–	–3.42	–0.01
Tb II	1(syn)	<–3.20	–	–3.48	–0.07
Dy II	2(syn)	–2.40	0.1	–3.54	–0.13
Er II	1(syn)	–2.56	–	–3.49	–0.08
Tm II	1(syn)	<–3.50	–	–3.50	–0.09
Yb II	1	–2.10	–	–3.18	0.23
Hf II	2(syn)	–2.00	0.1	–2.88	0.53
W I	1(syn)	<–1.50	–	–2.61	0.78
Pb I	2(syn)	0.10	0.2	–1.90	1.49

$^{12}C/^{13}C = 4 \pm 1$.

However, because the carbon isotopic ratio is low ($^{12}C/^{13}C = 4$), it is unlikely that C has retained its initial value in the envelope of CS 30322-023. As further discussed in Sect. 7, the combination of a low $^{12}C/^{13}C$ ratio and large N overabundance strongly suggests that pollution of the atmosphere by material processed by the CN cycle has occurred. In this respect, it is worth noting that CS 30322-023 falls among the other CEMP stars in a diagram showing [(C+N)/H] as a function of metallicity (Fig. 14). The α-elements in CS 30322-023 do not exhibit any overabundances with respect to the values expected for its metallicity from galactic chemical evolution. There is also no observed enhancement of r-process elements, whereas the s-process elements belonging to the second and third peaks are clearly enhanced (Fig. 15). Tc I and Tc II lines have been searched for, and not found. As

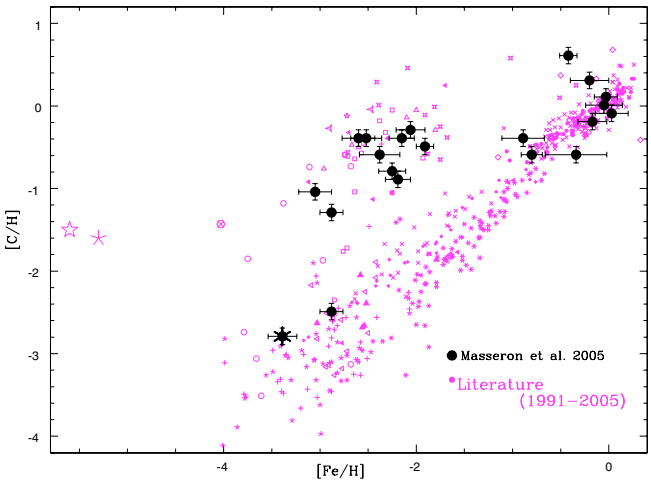

Fig. 11. [C/H] as a function of metallicity for metal-poor stars, collected from the literature (see Masseron 2006, for detailed references). The lower diagonal sequence corresponds to the trend expected from galactic chemical evolution for unpolluted stars. Two of the stars from the sample of Masseron (2006), among which are CS 30322-023 (asterisk), fall on this galactic sequence. The picture changes, however, when considering C+N (Fig. 14).

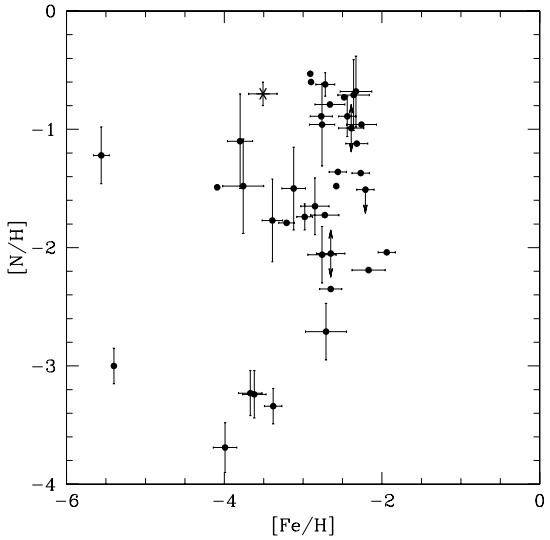

Fig. 12. Same as Fig. 11 for [N/H] as a function of metallicity for CEMP stars collected from the literature (see Sect. 4 for the full reference list). As usual, CS 30322-023 is represented by an asterisk.

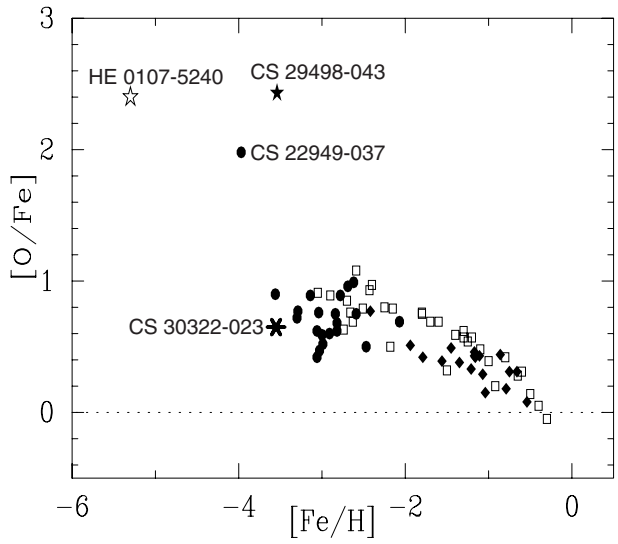

Fig. 13. [O/Fe] as a function of [Fe/H] for CS 30322-023 (asterisk), CS 29498-043 (Aoki et al. 2004), HE 0107-5240 (Bessell et al. 2004) and for unevolved dwarf stars from Israelian et al. (2001) (open squares), Cayrel et al. (2004) (filled circles), and Nissen et al. (2002) (filled diamonds). The filled symbols correspond to [O/Fe] values derived from the [O I] line, while open symbols correspond to oxygen abundances derived from the triplet or OH lines. No 3D corrections have been applied. Figure adapted from Aoki et al. (2004).

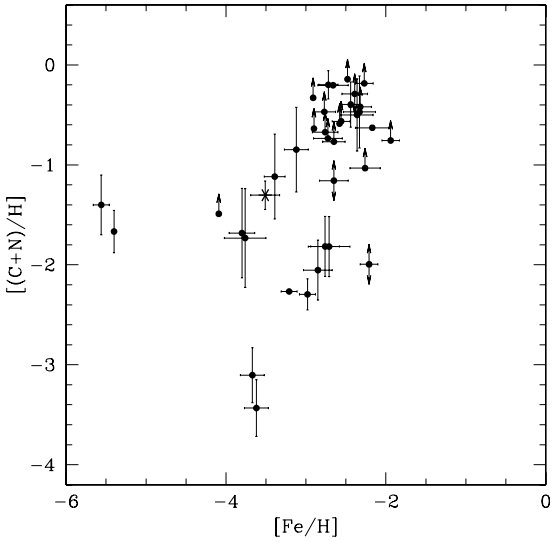

Fig. 14. [(C+N)/H] as a function of metallicity for the same sample of CEMP stars as in Fig. 12.

shown in Fig. 16, an upper limit $\log \epsilon(\mathrm{Tc}) < -1.4$ (translating to $\epsilon(\mathrm{Tc})/\epsilon(\mathrm{Zr}) < 0.2$) may be derived from the Tc I λ426.23 nm line. This upper limit on the Tc abundance is not meaningful, however, since $\epsilon(\mathrm{Tc})/\epsilon(\mathrm{Zr}) \sim 0.001$ is expected from s-process nucleosynthesis (see Fig. 15 of Goriely & Mowlavi 2000). The difficulty of detecting the Tc I line in this star results from its rather high temperature (as compared to solar-metallicity AGB stars, which are much cooler), implying that Tc is mostly ionized. Unfortunately, the strongest Tc II lines lie in the far ultraviolet; perhaps these lines could be searched for from space in the future.

The abundance pattern for heavy elements is presented in Fig. 15, along with the scaled solar r-process abundance pattern, and an s-process abundance pattern expected from proton-mixing, forming a ^{13}C pocket below the He-H discontinuity in a 0.8 $M_\odot$ AGB star of metallicity [Fe/H] = −3.8 (Goriely & Mowlavi 2000). With the exception of Sr and Y, all observed abundances almost perfectly match the predictions of a pure s-process operating at low metallicity in the framework of the proton-mixing scenario (Straniero et al. 1995; Goriely & Mowlavi 2000). The s-process abundance pattern in CS 30322-023 is at the lowest metallicity observed to date. As expected, it differs from its solar-metallicity counterpart due to the large Pb overabundance (Goriely & Mowlavi 2000; Busso et al. 2001; Goriely & Siess 2001), which matches the value observed in CS 30322-023 (Figs. 15 and 17), thus making this star a new member of the class of lead stars (Van Eck et al. 2001, 2003). The large spread in the Pb abundances observed among CEMP stars (Fig. 17) is surprising, however, as is further discussed in Sect. 7. The parameter responsible for this

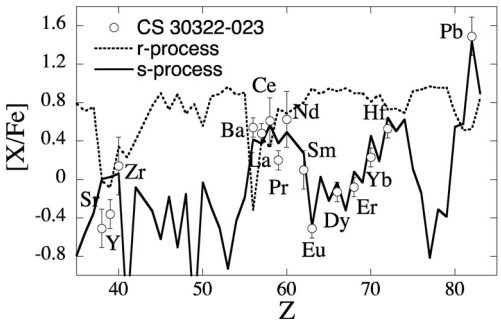

Fig. 15. Abundance pattern of CS 30322-23 compared to two model predictions for the s- and r-processes. The s-process abundance pattern has been computed by post-processing an AGB model of mass 0.8 $M_{\odot}$ and metallicity [Fe/H] = −3.8, as described in Goriely & Mowlavi (2000). The r-process pattern corresponds to the scaled solar r-process abundances, from Palme & Beer (1994).

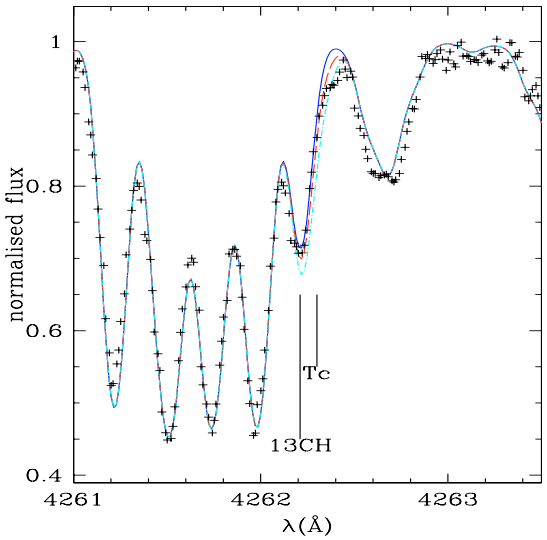

Fig. 16. The observed spectrum of CS 30322-023 (crosses) around the Tc I λ426.23 nm line, with three synthetic spectra: without Tc (blue solid line), with $\log \epsilon(\mathrm{Tc}) = -1.4$ (red dashed line), and with $\log \epsilon(\mathrm{Tc}) = -1.0$ (cyan dot-dashed line).

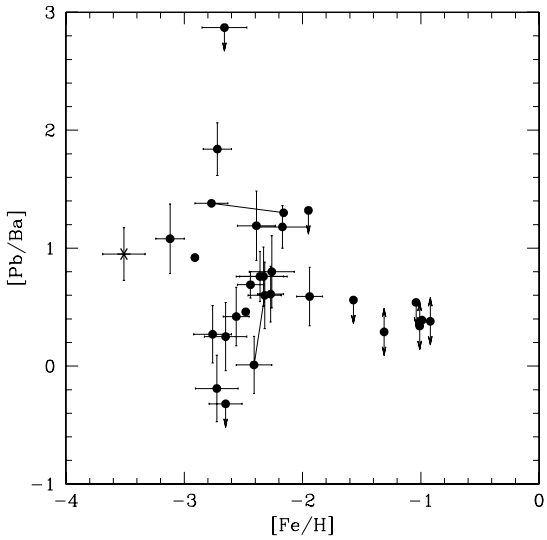

Fig. 17. The [Pb/Ba] ratio as a function of metallicity for the sample of CEMP stars (excluding r-process-enhanced stars) taken from the literature (see the references listed in Sect. 4). As before, CS 30322-023 is represented by an asterisk.

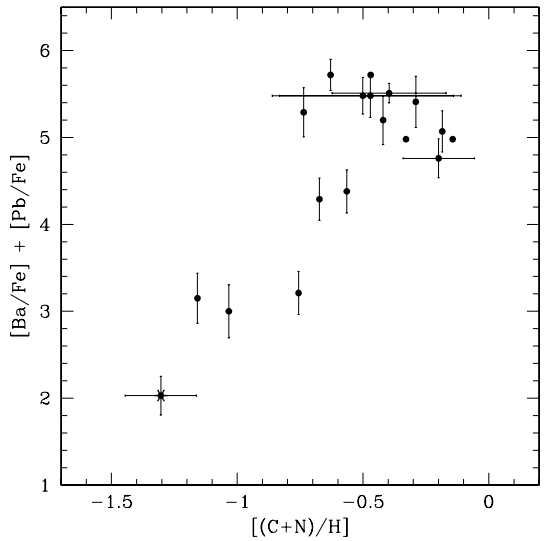

Fig. 18. The global overabundance of s-process elements in CEMP stars (excluding r-process-enhanced stars), expressed in terms of [Ba/Fe] + [Pb/Fe], as a function of [(C+N)/H]. Although the general trend may be explained by the dilution of the processed material in the envelope, there remains a significant – unexplained – scatter in the s-process abundances (at a given [(C+N)/H]).

scatter remains unidentified, as the scatter does not correlate with either [C/Fe] or N/(C+N).

To estimate the global overabundance of s-process elements in CEMP stars – when evaluating, for instance, its possible correlation with the C and N abundances – it is important to consider not only overabundances of elements (such as Ba) belonging to the second s-process peak, but also overabundances of elements (such as Pb) from the third peak. Failure to do so would largely underestimate the s-process overabundance whenever lead stars are involved. This is very clear from Fig. 15. Figure 18 reveals that there is indeed a general tendency for ([Ba/Fe] + [Pb/Fe]) to increase with [(C+N)/H] (this trend may in fact be ascribed to the dilution of the processed material in a more or less massive envelope), although there remains a considerable scatter. On the contrary, [(C+N)/H] exhibits little correlation with the s-process efficiency expressed in terms of [Pb/Ba] (Fig. 19).

In absolute terms, the s-process overabundance ([Ba/Fe] + [Pb/Fe]) in CS 30322-023 is thus moderate, when compared to other CEMP stars (Fig. 18), which is suggestive of a large dilution factor of the processed material in the envelope.

Considering the sum Ba+Pb, instead of solely Ba, is also of interest when discussing the [Ba/Eu] ratio. Figure 20 shows that, in a [Ba/Eu] vs. [C/Fe] diagram, there are several stars with [Ba/Eu] ratios that are intermediate between the solar s-process and solar r-process ratios. These stars have been coined "s+r" or "s/r" stars (Hill et al. 2000; Cohen et al. 2003a; Sivarani et al. 2004; Barbuy et al. 2005; Ivans et al. 2005; Jonsell et al. 2006); their [Ba/Eu] ratios do indeed seem peculiar when compared to the solar s-process ratio (Fig. 20). Detailed s-process computations in low-metallicity AGB stars (Goriely & Siess 2006) have shown that the [Ba/Eu] ratio predicted under such circumstances are quite different from the solar s-process Ba/Eu ratio (upper panel of Fig. 20), and matches at least some of the observed [Ba/Eu] values. When considering the [(Ba+Pb)/Eu] ratio, instead of the [Ba/Eu] ratio, s-process predictions become more robust (in the sense that the different environments yield similar

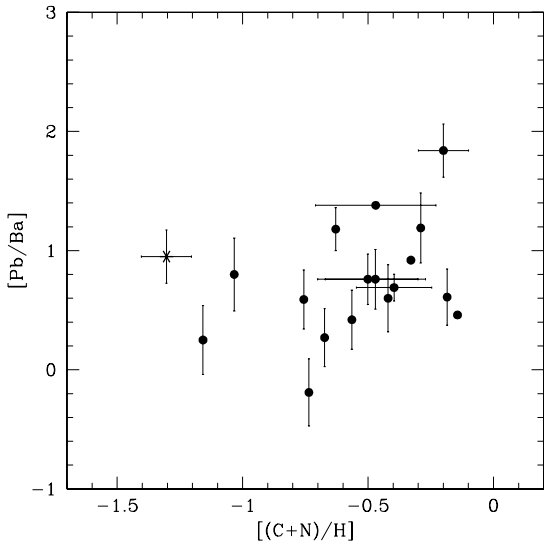

Fig. 19. Same as Fig. 17 for [Pb/Ba] as a function of [(C+N)/H].

values, within 0.6 dex). Such predictions may account for some of the stars displayed in the lower panel of Fig. 20, but the need for a separate class of "s+r" ("s/r") stars is even stronger, as they separate even more clearly from pure s- and pure r-stars when considering [(Ba+Pb)/Eu] instead of [Ba/Eu].

7. Observed abundances and possible models

In solar-metallicity AGB stars, C is brought to the surface by the third dredge-up, hence the C/O ratio for a given star is expected to increase steadily with time. Nitrogen is not enhanced, unless the operation of hot-bottom burning (HBB) in intermediate-mass AGB stars has converted C into N. The situation in low-metallicity AGB stars is not as simple, as several specific mixing processes with potentially large impact on the surface abundances have been found to operate in these stars. Since CS 30322-023 is believed to be a low-mass, extremely low-metallicity TP-AGB star, as we have argued in Sect. 5, we now briefly describe the various mixing processes in low-metallicity stars that have been specifically discussed in the literature:

- Some deep mixing is believed to occur in low-mass, low-metallicity stars on the first giant branch, after the luminosity bump. This deep mixing brings to the surface hydrogen-burning ashes, including Na and Al in some instances, and is a signature of hot hydrogen burning (Charbonnel 1994, 1995; Spite et al. 2006);
- He-flash-driven deep mixing (He-FDDM) occurs at the tip of the RGB when the helium-flash convective zone extends into the tail of the H-burning shell (Fujimoto et al. 1990; Hollowell et al. 1990; Fujimoto et al. 2000; Schlattl et al. 2001, 2002; Iwamoto et al. 2004; Suda et al. 2004). The injection of protons in the region of He-burning produces a H-flash and causes the convective region to split. The lower convective shell is powered by He burning while the upper one is driven by H burning. The structural readjustment subsequent to the H-flash leads to a CN-strong star, through the merging of the H-driven convective shell (formerly polluted with 3α–^{12}C) with the outer envelope. It is important to note, however, that the atmosphere of such a CN-strong star is not expected to be enriched in s-process elements. If the injection of protons in the He flash leads to the production of ^{13}C, and subsequently of s-elements, these heavy elements will remain trapped in the He-burning convective region, which the envelope never penetrates;
- very similar to the previous scenario is the mixing of protons into the thermal pulse at the beginning of the TP-AGB phase, which also leads to a CN-strong star (Fujimoto et al. 2000; Suda et al. 2004). In contrast with the previous situation, however, this process might produce s-process elements, but this needs to be confirmed (Aikawa, priv. comm.);
- "carbon injection" is a mixing process encountered exclusively in $Z = 0$ models (Chieffi et al. 2001; Siess et al. 2002). It occurs at the end of the early AGB phase when the

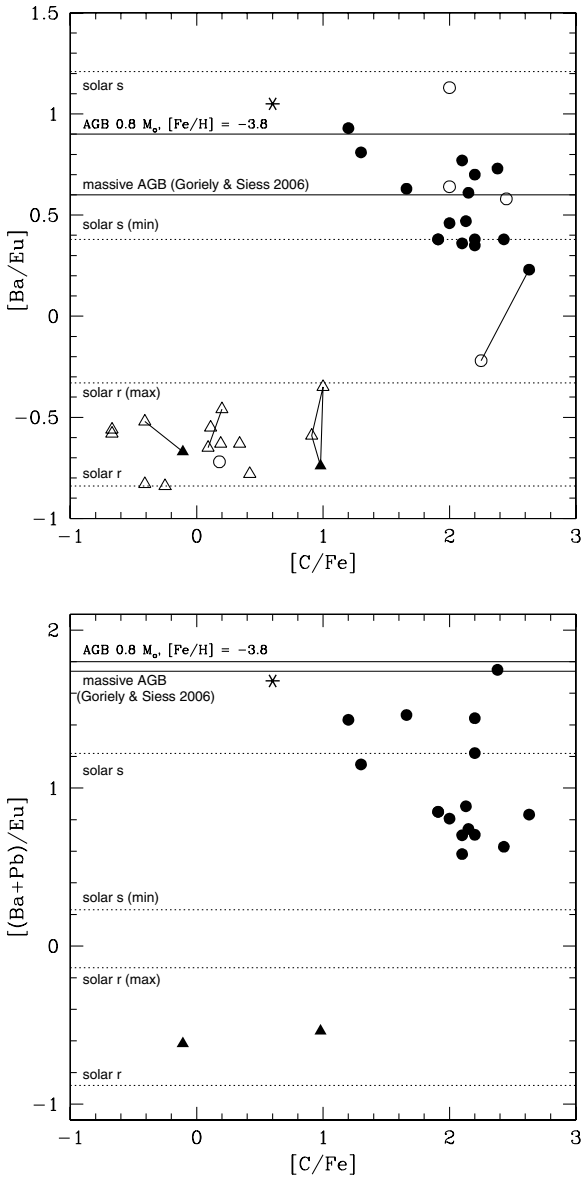

Fig. 20. *Upper panel*: [Ba/Eu] as a function of [C/Fe]. *Lower panel*: [(Ba+Pb)/Eu] as a function of [C/Fe]. Triangles: r-process-enhanced stars; circles: s-process-enhanced stars; asterisk: CS 30322-023. Open symbols correspond to stars with either no Pb data or with only an upper limit available. The solar [Ba/Eu] and [Pb/Eu] ratios ascribed to the r- and s-processes (from Goriely 1999) are displayed as dotted lines, along with the maximum r-process and minimum s-process solar ratios, taken from Table 3 of Goriely (1999). Predictions from the 0.8 $M_{\odot}$, [Fe/H] = −3.8 model (see Fig. 15) and from the s-process operating in massive AGB stars (from Fig. 6 of Goriely & Siess 2006) are also shown.

He-burning shell (He-BS), while approaching the hydrogen-burning shell, is subject to small- amplitude instabilities. In this process, after the development of a weak thermal pulse in the He-BS, a secondary convective zone forms at the He-H discontinuity. It grows in mass, penetrates downwards into the C-rich layers left over from the pulse, and initiates a H-flash by activation of CNO reactions. The subsequent structural readjustment causes the envelope to penetrate in this secondary convective zone, leading to a surface CN-enrichment;

– the "classical" proton-mixing scenario assumes that some extra mixing takes place at the base of the convective envelope during the third dredge-up. It is responsible for the injection of protons into the C-rich layers left by the pulse, leading to the formation of a ^{13}C pocket. The radiative burning of ^{13}C during the interpulse phase then leads to the production of s-process elements which, after passing through the pulse, are brought to the surface by the third dredge-up (Straniero et al. 1995; Goriely & Mowlavi 2000).

In addition to these extra-mixing mechanisms, HBB can also significantly modify the observed surface abundances, at least in intermediate-mass stars, when H-burning occurs at the base of the convective envelope, and partly converts ^{12}C into ^{14}N. HBB can also activate the NeNa and MgAl chains, and therefore could be responsible for ^{23}Na and ^{27}Al enrichment. In Pop III stars, HBB can be activated in stars with masses as low as $M \approx 2\ M_{\odot}$ (Siess et al. 2002).

Signatures of these mixing and HBB processes generally are a combined enhancement of hydrogen-burning products (low ^{12}C/^{13}C, high N, and sometimes high Na) *and* helium-burning products (^{12}C and possibly s-process elements) in the stellar envelope. Since the stellar envelope is enriched by primary ^{12}C, C-enhancement factors of several dex are expected. For example, in the 0.8 $M_{\odot}$ model described above, mixing between the He-flash and the stellar envelope increases the envelope carbon content to [C/H] $\simeq$ +1.0. Such large overabundances are not confirmed by observations thus far (see Fig. 11). The abundances in CS 30322-023 are instead suggestive of CN-cycling of formerly C-rich matter, perhaps through HBB. Since HBB is not expected to occur in a 0.8 $M_{\odot}$ star, we are thus left with the following alternatives. Either some extra mixing occurs in low-mass stars that results in H-burning similar to HBB, or an enrichment by an intermediate-mass AGB companion which has undergone HBB has polluted the presently-observed star. The latter suggestion must await firm evidence for orbital motion, which is lacking at present.

Further constraints on the the nucleosynthetic history of this star come from the s-process enrichment observed in CS 30322-023. The s-process in AGB stars is so far understood by the partial mixing of protons in C-rich layers, followed by the 3DUP of this material (Straniero et al. 1995; Goriely & Mowlavi 2000). As shown in Fig. 15, the CS 30322-023 s-process abundance pattern is in excellent agreement with the so-called partial-mixing model. However, in such a scenario, the s-process surface enrichment is inevitably accompanied by a large C enrichment due to the 3DUP of primary C made in the thermal pulse, in contradiction to the low C-to-s-process overabundance exhibited by CS 30322-023. None of the present s-process models could possibly explain such a ratio; for this reason CS 30322-023 is quite similar to the C-poor s-rich post-AGB star V453 Oph observed by Deroo et al. (2005).

More generally, the observed relation between the [Pb/Ba] ratio and metallicity shown in Fig. 17 is not reproduced by any current models. The traditional proton-mixing scenario (Goriely & Mowlavi 2000) cannot explain the low [Pb/Ba] stars observed at low metallicity, whereas the mixing of protons in the thermal pulse at the beginning of the TP-AGB phase, according to the models of Fujimoto et al. (2000) and Suda et al. (2004), predicts a more complicated trend between [Fe/H] and [Pb/Ba], not seen in Fig. 17 (compare with Fig. 7 of Suda et al. 2004).

Our new observation, as well as the C-poor, s-rich post-AGB star of Deroo et al. (2005), clearly show that our understanding of the mixing mechanism(s) that are responsible, not only for the surface enrichment, but also for more specific nucleosynthesis events such as the s-process, are still far from being under control. Our ability to quantitatively explain the existing observations remains highly dependent on stellar modeling, and most of all on the description of convective boundaries where some extra mixing takes place. A better description of the internal transport processes must also be accompanied with better knowledge of the mass loss, which indirectly influences the thermodynamical conditions at the base of the convective envelope and consequently the 3DUP events.

8. Summary

The star CS 30322-023 appears to be the most metal-poor ([Fe/H] = −3.5) s-process-rich star known so far. It is also a lead star, with [Pb/Ba] = +0.95. An LTE analysis of the Fe I/Fe II ionization balance yields a very low gravity of $\log g = -0.3$. Although it is likely that such an LTE analysis underestimates the gravity, a comparison with other CEMP stars analyzed with the LTE assumption reveals that CS 30322-023 is the most evolved example among known extremely metal-poor stars. It is most likely to be a low-mass (∼0.8 $M_{\odot}$) TP-AGB star. Larger masses would put CS 30322-023 too far (>20 kpc) in the outskirsts of the halo, where no recent star formation is expected. Despite the rather short lifetime of the TP-AGB phase, the high luminosity of TP-AGB stars makes it possible to sample them in a very large volume. The probability to uncover such low-mass, low-metallicity TP-AGB stars is therefore not small, as confirmed by a detailed quantitative analysis. We thus expect that additional examples will be revealed in the near future, as spectroscopic surveys of the Galaxy push to ever fainter limiting magnitudes.

The observed abundance pattern of CS 30322-023 is, however, quite puzzling, in that it exhibits s-process elements without a strong C overabundance, as would be expected if the s-process operates in a He-burning environment. The light-element abundance pattern is instead reminiscent of the operation of the CN cycle (strong N overabundance, low ^{12}C/^{13}C ratio, Na overabundance). Hot-bottom burning is not expected to operate in such low-mass stars. We therefore suggest that the enrichment of the envelope with nuclear-burning products does not result from the traditional third dredge-up events, but rather may be caused by some mixing mechanism that has yet to be identified. Although there is no firm evidence at present for orbital motion of this star, an alternative possibility is that CS 30322-023 resides in a binary system, and has been polluted by matter from an intermediate-mass companion that produced s-process elements and converted C into N during HBB episodes. Clearly, full understanding of the abundance pattern and apparent evolutionary state of CS 30322-023 will depend on future high-resolution studies of stars with similar characteristics. Abundance determinations duly accounting for NLTE and 3D effects, which are suspected to play an important role in metal-poor giant stars, should as well bring progress in this field.

Acknowledgements. We thank J. Johnson, S. Lucatello and M. Spite for providing us with supplementary radial-velocity measurements, N. Christlieb for a critical reading of the manuscript, and C. Laporte for help with a preliminary abundance analysis of CS 30322-023. D. Pourbaix provided help with the orbit search. T.C.B. acknowledges partial funding for this work from grants AST 00-98508, AST 00-98549, and AST 04-06784, as well as from grant PHY 02-16783: Physics Frontiers Center/Joint Institute for Nuclear Astrophysics (JINA), all from the U.S. National Science Foundation. The *Fonds National de la Recherche Scientifique* (F.N.R.S., Belgium) supported the research presented in this paper, since S.vE., S.G. and L.S. are F.N.R.S. Research Associates, A.J. is Senior Research Associate and B.F. is Scientific Research Worker.

References

Alonso, A., Arribas, S., & Martinez-Roger, C. 1998, A&AS, 131, 209
Alonso, A., Arribas, S., & Martínez-Roger, C. 1999, A&AS, 140, 261
Alvarez, R., Mennessier, M.-O., Barthes, D., Luri, X., & Mattei, J. A. 1997, A&A, 327, 656
Alvarez, R., Jorissen, A., Plez, B., et al. 2001, A&A, 379, 305
Aoki, W., Ryan, S. G., Norris, J. E., et al. 2001, ApJ, 561, 346
Aoki, W., Ando, H., Honda, S., et al. 2002a, PASJ, 54, 427
Aoki, W., Norris, J. E., Ryan, S. G., Beers, T. C., & Ando, H. 2002b, ApJ, 576, L141
Aoki, W., Norris, J. E., Ryan, S. G., Beers, T. C., & Ando, H. 2002c, ApJ, 567, 1166
Aoki, W., Ryan, S. G., Norris, J. E., et al. 2002d, ApJ, 580, 1149
Aoki, W., Norris, J. E., Ryan, S. G., et al. 2004, ApJ, 608, 971
Aoki, W., Ryan, S. G., Iwamoto, N., et al. 2003, ApJ, 592, L67
Arenou, F., Grenon, M., & Gómez, A. 1992, A&A, 258, 104
Asplund, M. 2005, ARA&A, 43, 481
Asplund, M., Grevesse, N., & Sauval, A. J. 2005, in Cosmic Abundances as Records of Stellar Evolution and Nucleosynthesis, ed. T. G. Barnes III, & F. N. Bash (San Francisco: ASP), ASP Conf. Ser., 336, 25
Bahcall, J. N., & Soneira, R. M. 1980, ApJS, 44, 73
Barbuy, B., Spite, M., Spite, F., et al. 2005, A&A, 429, 1031
Beers, T. C., & Christlieb, N. 2005, ARA&A, 43, 531
Beers, T. C., Preston, G. W., & Shectman, S. A. 1985, AJ, 90, 2089
Beers, T. C., Preston, G. W., & Shectman, S. A. 1992, AJ, 103, 1987
Bessell, M. S., Christlieb, N., & Gustafsson, B. 2004, ApJ, 612, L61
Burstein, D., & Heiles, C. 1982, AJ, 87, 1165
Busso, M., Gallino, R., Lambert, D. L., Travaglio, C., & Smith, V. V. 2001, ApJ, 557, 802
Cayrel, R., Depagne, E., Spite, M., et al. 2004, A&A, 416, 1117
Charbonnel, C. 1994, A&A, 282, 811
Charbonnel, C. 1995, ApJ, 453, L41
Chieffi, A., Domínguez, I., Limongi, M., & Straniero, O. 2001, ApJ, 554, 1159
Christlieb, N., Green, P. J., Wisotzki, L., & Reimers, D. 2001, A&A, 375, 366
Christlieb, N., Bessell, M. S., Beers, T. C., et al. 2002, Nature, 419, 904
Cohen, J. G., Persson, S. E., Elias, J. H., & Frogel, J. A. 1981, ApJ, 249, 481
Cohen, J. G., Christlieb, N., Qian, Y.-Z., & Wasserburg, G. J. 2003a, ApJ, 588, 1082
Cohen, M., Wheaton, W. A., & Megeath, S. T. 2003b, AJ, 126, 1090
Cohen, J. G., Christlieb, N., McWilliam, A., et al. 2004, ApJ, 612, 1107
Cutri, R., Skrutskie, M., Van Dyk, S., et al. 2003, The Two Micron All Sky Survey Catalog of Point Sources
Dearborn, D. S. P., Liebert, J., Aaronson, M., et al. 1986, ApJ, 300, 314
Deroo, P., Reyniers, M., van Winckel, H., Goriely, S., & Siess, L. 2005, A&A, 438, 987
Frebel, A., Aoki, W., Christlieb, N., et al. 2005, Nature, 434, 871
Frebel, A., Aoki, W., Christlieb, N., et al. 2006, in From Lithium to Uranium: Elemental Tracers of Stellar Evolution, ed. V. Hill, P. François, & F. Primas (Cambridge University Press), IAU Symp., 228, 207
Fujimoto, M. Y., Iben, I. J., & Hollowell, D. 1990, ApJ, 349, 580
Fujimoto, M. Y., Ikeda, Y., & Iben, I. J. 2000, ApJ, 529, L25
Goriely, S. 1999, A&A, 342, 881
Goriely, S., & Mowlavi, N. 2000, A&A, 362, 599
Goriely, S., & Siess, L. 2001, A&A, 378, L25
Goriely, S., & Siess, L. 2006, in From Lithium to Uranium: Elemental Tracers of Stellar Evolution, ed. V. Hill, P. François, & F. Primas (Cambridge University Press), IAU Symp., 228, 451
Gratton, R. G., Sneden, C., Carretta, E., & Bragaglia, A. 2000, A&A, 354, 169
Groenewegen, M. A. T., Smith, C. H., Wood, P. R., Omont, A., & Fujiyoshi, T. 1995, ApJ, 449, L119
Gustafsson, B., Edvardsson, B., Eriksson, K., et al. 2003, in Stellar Atmosphere Modeling, ed. I. Hubeny, D. Mihalas, & K. Werner (San Francisco: ASP), ASP Conf. Ser., 288, 331
Hill, V., Barbuy, B., Spite, M., et al. 2000, A&A, 353, 557
Hill, V., Plez, B., Cayrel, R., et al. 2002, A&A, 387, 560
Hollowell, D., Iben, I. J., & Fujimoto, M. Y. 1990, ApJ, 351, 245
Honda, S., Aoki, W., Kajino, T., et al. 2004, ApJ, 607, 474
Israelian, G., Rebolo, R., García López, R. J., et al. 2001, ApJ, 551, 833
Israelian, G., Shchukina, N., Rebolo, R., et al. 2004, A&A, 419, 1095
Ivans, I. I., Sneden, C., Gallino, R., Cowan, J. J., & Preston, G. W. 2005, ApJ, 627, L145
Iwamoto, N., Kajino, T., Mathews, G. J., Fujimoto, M. Y., & Aoki, W. 2004, ApJ, 602, 377
Johnson, J. A. 2002, ApJS, 139, 219
Johnson, J., & Bolte, M. 2002, ApJ, 579, L87
Johnson, J. A., & Bolte, M. 2004, ApJ, 605, 462
Jonsell, K., Barklem, P. S., Gustafsson, B., et al. 2006, A&A, 451, 651
Jorissen, A. 2003, in Asymptotic Giant Branch Stars, ed. H. Habing, & H. Olofsson (New York: Springer Verlag), 461
Korn, A. J., Shi, J., & Gehren, T. 2003, A&A, 407, 691
Kroupa, P. 2001, MNRAS, 322, 231
Kudritzki, R., Pauldrach, A., & Puls, J. 1987, A&A, 173
Kudritzki, R. P., Pauldrach, A. W. A., Puls, J., & Voels, S. R. 1991, in The Magellanic Clouds, ed. R. Haynes, & D. Milne (Dordrecht: Kluwer), IAU Symp., 148, 279
Lucatello, S., Gratton, R., Cohen, J. G., et al. 2003, AJ, 125, 875
Masseron, T. 2006, Ph.D. Thesis (Observatoire de Paris)
Masseron, T., Plez, B., Primas, F., Van Eck, S., & Jorissen, A. 2005, in 13th Cambridge Workshop on Cool Stars, Stellar Systems and the Sun, ed. F. Favata [arXiv:astro-ph/0601253]
Masseron, T., Plez, B., Primas, F., Van Eck, S., & Jorissen, A. 2006, in From Lithium to Uranium: Elemental Tracers of Stellar Evolution, ed. V. Hill, P. François, & F. Primas (Cambridge University Press), IAU Symp., 228, 219
Mauron, N., Azzopardi, M., Gigoyan, K., & Kendall, T. R. 2004, A&A, 418, 77
Mauron, N., Kendall, T. R., & Gigoyan, K. 2005, A&A, 438, 867
McWilliam, A., Preston, G. W., Sneden, C., & Searle, L. 1995, AJ, 109, 2757
Nissen, P. E., Primas, F., Asplund, M., & Lambert, D. L. 2002, A&A, 390, 235
Norris, J. E., Ryan, S. G., & Beers, T. C. 1997a, ApJ, 488, 350
Norris, J. E., Ryan, S. G., & Beers, T. C. 1997b, ApJ, 489, L169
Norris, J. E., Ryan, S. G., & Beers, T. C. 1999, ApJS, 123, 639
Norris, J. E., Ryan, S. G., & Beers, T. C. 2001, ApJ, 561, 1034
Palme, H., & Beer, H. 1994, in Landolt-Börnstein, New Series, Group VI, Vol. 3a, ed. H. H. Voigt (Berlin: Springer Verlag), 196
Plez, B., & Cohen, J. G. 2005, A&A, 434, 1117
Preston, G. W., & Sneden, C. 2001, AJ, 122, 1545
Reimers, D. 1975, Mem. Soc. Roy. Sci. Liège, 6th Ser., 8
Robin, A., Reylé, C., Derrière, S., & Picaud, S. 2003, A&A, 409, 523
Ryan, S. G., Norris, J. E., & Bessell, M. S. 1991, AJ, 102, 303
Schlattl, H., Cassisi, S., Salaris, M., & Weiss, A. 2001, ApJ, 559, 1082
Schlattl, H., Salaris, M., Cassisi, S., & Weiss, A. 2002, A&A, 395, 77
Schmidt-Kaler, T. 1982, in Landolt-Börnstein, New Series, Vol. VI/2b, ed. K. H. Hellwege (Berlin: Springer Verlag), 1
Shchukina, N. G., Bueno, J. T., & Asplund, M. 2005, ApJ, 618, 939
Siess, L. 2006, A&A, 448, 717
Siess, L., Livio, M., & Lattanzio, J. 2002, ApJ, 570, 329
Simmerer, J., Sneden, C., Cowan, J. J., et al. 2004, ApJ, 617, 1091
Sivarani, T., Bonifacio, P., Molaro, P., et al. 2004, A&A, 413, 1073
Šleivyte, J., & Bartkevičius, A. 1990, Vilnius Astron. Observ. Bull., 85, 3
Sneden, C., Cowan, J. J., Burris, D. L., & Truran, J. W. 1998, ApJ, 496, 235
Sneden, C., Cowan, J. J., Ivans, I. I., et al. 2000, ApJ, 533, L139
Sneden, C., Preston, G. W., & Cowan, J. J. 2003, ApJ, 592, 504
Spite, M., Cayrel, R., Hill, V., et al. 2006, A&A, 455, 291, (First stars IX)
Straniero, O., Gallino, R., Busso, M., et al. 1995, ApJ, 440, L85
Suda, T., Aikawa, M., Machida, M. N., Fujimoto, M. Y., & Iben, I. J. 2004, ApJ, 611, 476
Thévenin, F., & Idiart, T. P. 1999, ApJ, 521, 753
Travaglio, C., Gallino, R., Busso, M., & Gratton, R. 2001, ApJ, 549, 346
Van Eck, S., Goriely, S., Jorissen, A., & Plez, B. 2001, Nature, 412, 793
Van Eck, S., Goriely, S., Jorissen, A., & Plez, B. 2003, A&A, 404, 291
van Loon, J. T. 2000, A&A, 354, 125
van Loon, J. T. 2006, in Stellar Evolution at Low Metallicity: Mass Loss, Explosions, Cosmology, ed. H. Lamers, N. Langer, T. Nugis, & K. Annuk, ASP Conf. Ser., in press
Vassiliadis, E., & Wood, P. R. 1993, ApJ, 413, 641
Weiss, A., Schlattl, H., Salaris, M., & Cassisi, S. 2004, A&A, 422, 217
Westin, J., Sneden, C., Gustafsson, B., & Cowan, J. J. 2000, ApJ, 530, 783